Optical conductivity studies in a one-dimensional organic metal: Tetrathiofulvalene tetracyanoquinodimethan (TTF) (TCNQ)†

A. A. Bright,* A. F. Garito, and A. J. Heeger

Department of Physics and Laboratory for Research on the Structure of Matter, University of Pennsylvania, Philadelphia, Pennsylvania 19174

(Received 3 December 1973)

The optical properties of tetrathiofulvalene tetracyanoquinodimethan (TTF) (TCNQ) are reported in the visible and near infrared from room temperature to 4.2 K. The experimental results are analyzed in terms of simple Drude theory, with corrections made for anisotropic effects introduced by the anisotropic band structure. The inclusion of a frequency dependence in the electron scattering time is found to be unnecessary. The reflectance spectrum for polarization parallel to the conducting axis shows a plasma edge at about 1.4 μm. The plasma frequency is used to infer a value for the effective mass and the tight-binding transfer integral ($t \simeq 0.1$ eV). The plasma frequency and the scattering time lead to a conductivity consistent with the measured room-temperature dc value. All of this information confirms that at room temperature, (TTF)(TCNQ) is a highly anisotropic (pseudo-one-dimensional) metal. Studies of the related materials (asymmetric TTF)(TCNQ) and (tetramethyl TTF)(TCNQ) show similar behavior. The temperature dependence of the scattering rate is found to be consistent with single-phonon scattering, with a contribution from temperature-independent defect scattering which varies from sample to sample and which increases as the number of defects increases. The defect scattering is used to obtain an estimate of the single-particle residual resistivity. Comparison with the typical dc data shows that the measured dc resistivity regularly falls below the residual resistivity by an order of magnitude, implying that the dc conductivity is carried in a collective manner. From the linear temperature dependence of τ^{-1}, a value is obtained for the dimensionless electron-phonon coupling constant $\lambda \simeq 1.3$.

I. INTRODUCTION

The organic charge-transfer salt tetrathiofulvalene tetracyanoquinodimethan [(TTF)(TCNQ)] has recently been the subject of considerable interest[1-3] because of the well-known predictions of dynamical instabilities occurring in one-dimensional metals. Measurements of the optical,[4,5] electrical,[6,7] and dielectric[8] anisotropies have demonstrated the pseudo-one-dimensionality of the electronic properties of (TTF)(TCNQ).

Standard four-probe dc[1,2] and microwave[8] measurements along the crystallographic b axis show that at room temperature, (TTF)(TCNQ) is the best organic conductor known, with a conductivity of nearly 10^3 $(\Omega\,\mathrm{cm})^{-1}$. With decreasing temperature, the conductivity rapidly increases to a maximum value which differs from crystal to crystal. Below the maximum near 58–60 K, the conductivity falls dramatically, characteristic of a metal-insulator transition.

A variety of experimental measurements have been performed in order to clarify the dominant interactions and obtain a measure of the over-all scale of energies involved. Estimates of the bandwidth were obtained from studies of the plasma frequency,[4,5,9] thermoelectric power,[10] and magnetic susceptibility.[7,11] In each case, a value of order 0.1 eV was found for the intrachain (b axis) transfer integral, indicating a bandwidth of order 0.5 eV. Information on the strength of the electron-electron interaction was obtained from magnetic-susceptibility[11] and nuclear-relaxation-rate studies.[12,13] The nonmagnetic ground state and nonenhanced susceptibility in the metallic state[12,13] demonstrated that Coulomb correlation effects play a minor role. Results from the conductivity studies, however, suggest a strong electron-phonon interaction. The mean free path is given by[14]

$$\Lambda = v_F \tau = \sigma \pi \hbar / 2 N e^2 a \,, \tag{1}$$

where N is the carrier density, a is the lattice constant in the conducting direction, and σ is the measured conductivity. With $a = 3.8$ Å,[15] $N = 4.7 \times 10^{21}$ cm^{-3}, and $\sigma = 10^3$ $(\Omega\,\mathrm{cm})^{-1}$, Λ is estimated to be of order 1 to 2 lattice constants. Thus the electrons are very strongly coupled to the lattice or molecular modes, and the system is near the limit of applicability of band theory. This has been confirmed by infrared reflectivity studies of the scattering rate,[4,5,9] τ_{ph}^{-1}. Using Hopfield's expression[16] for the dimensionless coupling constant

$$\lambda = \hbar / 2\pi k_B T \tau_{\mathrm{ph}} \tag{2}$$

(valid for $T > \Theta_D$), a strong coupling value of $\lambda \simeq 1.3$ was obtained.[4,9] This is developed thoroughly in this paper with measurements of the full temperature dependence of $\tau(T)$.

A pseudo-one-dimensional electronic system such as (TTF)(TCNQ) strongly coupled to the lattice is expected to be unstable toward a soft-mode structural instability driven by the divergent re-

sponse of the electron gas at $q = 2k_F$ (the Peierls instability).[1,17-19] Generally, one anticipates a decrease in conductivity due to increased scattering for a system undergoing such an instability. Thus the strong temperature dependence observed in the metallic state has been difficult to understand on the basis of single-particle scattering.

The fact that the conductivity above 58 K increases rapidly with decreasing temperature in all samples was interpreted as evidence for the presence of electron-electron correlations mediated by the soft phonons near $2k_F$.[1] This interpretation led Bardeen[20] to point out that indeed the correlations might result from the Peierls effect; however, the resultant dynamically distorted state could give enhanced conductivity arising from a coupled electron-phonon running-wave mechanism first described by Fröhlich.[18] In principle, the Fröhlich mechanism and BCS pairing could operate simultaneously, since they do not appear to be mutually exclusive.[21] Recently, Allender, Bray and Bardeen,[22] using a Ginsburg-Landau approach, have calculated a conductivity ratio of $\sigma/\sigma_{RT} \sim 20$, in agreement with values commonly found in (TTF)(TCNQ). However, their results are limited to temperatures outside the critical region, which they estimate as $\Delta T \sim 10$ K.

Experimental evidence of strong correlations and excess dc conductivity in the metallic state above 58 K has been obtained from several studies. The thermopower deviates from the simple linear behavior found at high temperatures and approaches zero at the transition.[10] Considering the thermopower as a measure of entropy per carrier indicates a reduced entropy in the metallic state and strong electron correlations in the temperature range ($58 < T < 140$ K) where the conductivity is maximum. Moreover, measurements of the temperature dependence of the scattering time, τ, from infrared reflectivity studies described in detail in this paper provide evidence of excess dc conductivity and independently suggest that the strong temperature dependence of the conductivity in all (TTF)(TCNQ) crystals arises not from single-particle scattering but from a collective many-body effect.

The experimental situation regarding the giant conductivity maximum has been controversial, since experimental questions associated with four-probe conductivity measurements in anisotropic materials have been raised[23] and studied.[6] Consequently, measurements of the electrical conductivity at infrared frequencies (in the Drude sense) become important, both in order to help clarify the intrinsic transport properties and also to provide an over-all understanding of the electronic properties of this interesting system.

In this paper, we report measurements of the optical properties of (TTF)(TCNQ) in the visible and near-infrared regions from room temperature to 4.2 K. Preliminary studies of the related materials *cis*(*trans*)-dimethyl tetrathiofulvalene TCNQ [(ATTF)(TCNQ)] and tetramethyltetrathiofulvalene TCNQ [(TMTTF)(TCNQ)] are also reported.

II. EXPERIMENTAL PROCEDURES

The preparation of TCNQ has been described elsewhere.[8,24] Tetrathiofulvalene (TTF) was prepared by treatment of 1,3-dithiolium hydrogen sulfate or percholorate with triethylamine.[25] The crude material was purified by multiple gradient sublimation (70 °C, 10^{-5} Torr). *Analysis*: calculated for $C_6S_4H_4$: C = 35.26, H = 1.98, S = 62.76; found: C = 35.25, H = 1.87, S = 62.71.

(TTF)(TCNQ) single crystals were grown by diffusion in a solution of acetonitrile. The (TTF)(TCNQ) crystals tended to grow in the form of flat needles, up to a few mm long.

Single crystals thin enough for optical-absorption measurements (i.e., a few μm thick) were selected by visual inspection. Attempts were made to cleave the crystals even thinner by placing them between two layers of scotch tape and peeling the tape apart. Although cleaving did occur, the crystals generally were fractured severely by this procedure, resulting in fragments too small to use. In addition, removal of the crystal fragments from the tape was difficult. No solvent was found which would dissolve the tape adhesive without attacking the crystals as well. Attempts to solvent polish crystals to reduce their thickness also failed due to the fragility of the material. It was concluded that only naturally grown crystals could be used for absorption measurements.

For reflectance measurements, large crystals with well-developed faces were selected visually. Polycrystalline samples were also made by compressing the material in a press at pressures up to 10 000 lb/in.^{2}. Adequate surface quality was obtained by polishing to optical flatness the surfaces of the press.

A microspectrophotometer was constructed[26] for measurements of the absorbance of single crystals of (TTF)(TCNQ) in the visible using a Beckman DK-2 as a monochromatic light source. The "sample" beam was brought out of the sample compartment with mirrors and passed through an adjustable diaphragm into a Leitz-Wetzlar polarizing transmission microscope fitted with a photomultiplier detector. The diaphragm could be either circular or a pair of crossed slits. An image of the diaphragm was focused on the sample by a 20× substage objective. The image was kept smaller than the sample in order to avoid light leaks past the sample. The transmitted light was passed through a 10× superstage objective, a rotatable

polarizer, and a second adjustable diaphragm, and was finally focused on the cathode of the photomultiplier tube. Both the field diaphragm and the sample were focused on the second diaphragm, which eliminated any light scattered past the sample into the measuring beam to better than 1 part in 10 000.

The absorbance was determined by measuring the transmittance of the sample at fixed wavelengths. The sample was moved in and out of the light path to measure the ratio of the signal levels. For samples uniform in thickness over an area large compared to the image of the field aperture, negligible error was introduced by the repeated movement of the sample.

The quality of the polarizer was checked by measuring the ratio of the signals obtained through a plastic polaroid when it was placed parallel and perpendicular to the polarizer. The ratio of 2000 to 1 obtained sets an upper limit of about 3.3 on the optical density that can be measured on a highly anisotropic sample in its strongly absorbing direction.

There are other subtle effects that limit the useful range of the instrument.[27] The convergence of the light beam from the objective onto the sample implies that the E vector of some of the incident light is not parallel to the surface of the sample. Thus extraneous signals corresponding to unwanted polarization directions can be mixed into the signal. A second effect results from light reflected back from the surface of the sample to the substage objective. This light may then be reflected to the superstage objective and then onto the top surface of the sample. It is impossible to mask this scattered light away except by placing the sample over a tiny pinhole. For the samples used in this experiment, such a masking technique was impossible. Consideration of these effects led to the conclusion that the maximum optical density the system was capable of measuring was approximately 3.0.

Reflectance of polycrystalline compactions was measured using a Perkin-Elmer model 421 spectrophotometer in the infrared and a Cary model 14 spectrophotometer in the visible and near infrared. Both instruments were equipped with specular reflectance accessories. Since the beam size of the Cary 14 was too large to allow measurements on single crystals, a specular reflectance attachment for the Beckman DK-2 was designed and constructed. The beam dimensions at the sample were 3×1.5 mm. The sample and reference paths were made identical. A reference mirror of silver or gold was used in the reference beam at the location corresponding to the sample. The instrument baseline was measured with a similar mirror replacing the sample. Both this mirror and the sample were mounted with vacuum grease onto a copper mask with pinholes up to 0.75 mm in diameter. The mask was painted with ultraflat black paint and was firmly attached to the cold end of the cryostat, an Air Products and Chemicals Helitran system.

Polarized spectra were obtained by placing plastic Polaroid material in both the sample and the reference beams. Special Polaroids were obtained for use from 0.85 to 2.2 μm.

III. EXPERIMENTAL RESULTS

The single-crystal visible absorption spectrum is shown in Fig. 1 for polarization perpendicular to the conducting crystallographic b axis. Even though the sample was approximately 2.5 μm thick, its optical density to light polarized parallel to the b axis was, at all wavelengths in this range, greater than 3.0, corresponding to an absorption coefficient α greater than 3×10^4 cm^{-1}. The transmittance was accurately proportional to $\sin^2\theta$, where θ is the polarization angle relative to the b axis as shown in Fig. 2. The measured anisotropy in the transmittance is greater than about 1000. The dc conductivity is similarly anisotropic with maximum conductivity along the b axis.[6-8]

The most significant aspect of the visible absorption, for the present purposes, is the extreme optical anisotropy. The strong absorption parallel to the conducting axis is clearly related to the metallic nature of the material in this direction. However, since the widths of the partially filled metallic bands in this system are on the order of a few tenths of an eV as inferred from magnetic-susceptibility,[11] nuclear-relaxation,[13] and thermoelectric-power[10] measurements, the absorption in

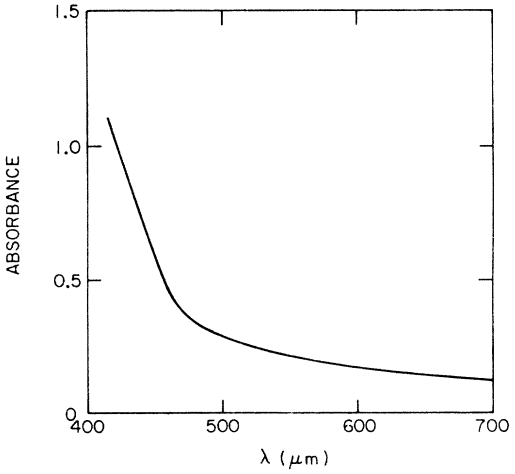

FIG. 1. Polarized absorption spectra of (TTF) (TCNQ) single crystals with E field perpendicular to the b axis. The absorption parallel to the conducting axis was too high to measure on this sample, which was 2.5 μm thick.

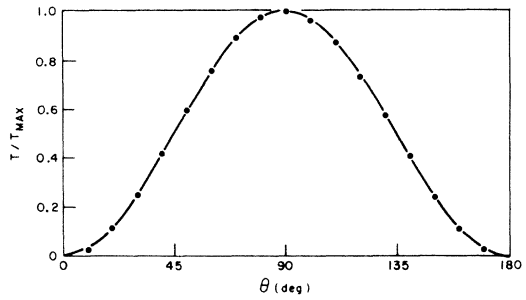

FIG. 2. Normalized transmittance of a (TTF) (TCNQ) single crystal as a function of polarization angle relative to the conducting b axis. The data points fall accurately on the $\sin^2\theta$ curve and indicate an anisotropy of greater than 10^3.

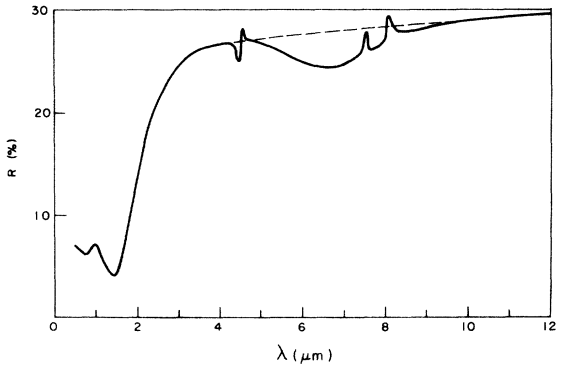

FIG. 4. Reflectance spectrum of a (TTF) (TCNQ) polycrystalline compaction. The structure from 5 to 8 μm arises from molecular vibrational modes.

the visible is most likely due to an interband transition. The absorption of perpendicularly polarized light, on the other hand, shows no unusual behavior. The spectrum is similar to those observed in insulating TCNQ salts.[28] This suggests that the optical properties in the infrared should be similarly anisotropic and can be expected to resemble those of metals for light polarized along the conducting axis, or insulators for perpendicularly polarized light.

In addition to (TTF)(TCNQ), TCNQ salts have been synthesized using the related molecules *cis* (*trans*)-dimethyl TTF (ATTF) and tetramethyl TTF (TMTTF). In these molecules, two or all four of the hydrogen atoms on the ends of the TTF molecules are replaced by methyl groups. Thin single crystals of (ATTF)(TCNQ) and (TMTTF)(TCNQ) were examined visually. Although no crystals could be found which were thin enough to allow accurate absorbance measurements to be made, crystals transparent to perpendicularly polarized light were examined with monochromatic light. Both materials appeared qualitatively similar to (TTF)(TCNQ). In addition, both materials had unmeasurably high absorbances for light polarized parallel to their conducting axes. It can be concluded that the addition of the methyl groups has relatively little effect on the optical properties of the compounds.

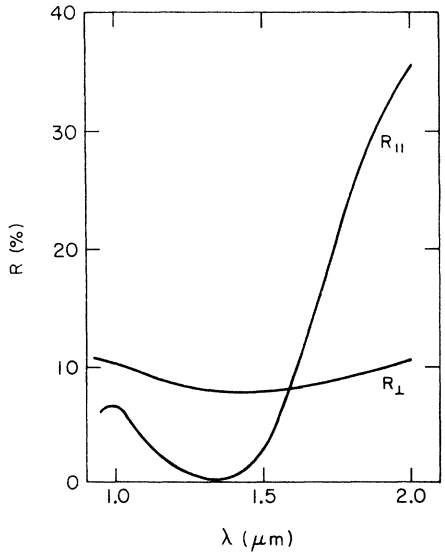

FIG. 3. Polarized single-crystal reflectance spectra of (TTF) (TCNQ) in the vicinity of the plasma edge.

The room-temperature near-infrared reflectance spectrum of a single crystal of (TTF)(TCNQ) is shown in Fig. 3 for light polarized parallel and perpendicular to the conducting axis. The spectra show the expected anisotropic behavior. The perpendicular reflectance is small and shows no interesting structure. The parallel reflectance, on the other hand, shows a plasma edge, with the reflectance rising from a minimum of less than 1% at 1.4 μm to a value of 34% at 2μm. In addition, there is a peak in the parallel reflectance at 1.0 μm which is not observed when the light is polarized perpendicular to the conducting axis.

The reflectance spectrum from 0.5 to 12 μm of a polycrystalline compaction of (TTF)(TCNQ) is shown in Fig. 4. The plasma edge is again clearly observable with a minimum reflectance at 1.4 μm. That this is in fact the plasma edge, in spite of the low-reflectance value at long wavelengths, is seen by noting that the anisotropic-single-crystal data indicate the one-dimensional nature of the electronic properties. The measured curve (Fig. 4) is an average over all crystalline orientations in the solid, while the metallic reflection is expected only in proportion to $\cos^2\theta$, where θ is the angle between the electric field vector of the radiation and the conducting axis. Thus, the measured long-wavelength reflectance of about 30% corresponds to near-total metallic reflection ($\langle\cos^2\theta\rangle = \frac{1}{3}$).

The component, $R_{\parallel}$, parallel to the conducting axis may be extracted from the data of Fig. 4 by subtracting the reflectance due to the transverse directions. This perpendicular reflectance is assumed constant in the infrared and equal to the minimum value at the plasma edge. The resultant curve, corrected for $\langle\cos^2\theta\rangle$, is shown in Fig. 5. The single-crystal data for $R_{\parallel}$ are shown as the dashed curve for comparison in the region of overlap. The spectrum clearly shows the plasma edge and metallic reflection in the infrared. There is in addition to the structure associated with the plasma edge, a weaker minimum in the reflectivity centered at 6 μm as well as several other sharper lines (Fig. 4). These lines are related to molecular vibrational modes and will be dealt with in a future publication.[29]

Figure 6 shows the infrared reflectance of compactions of (ATTF)(TCNQ) and (TMTTF)(TCNQ). The spectra resemble closely that of (TTF)(TCNQ). The plasma edge is observed in all three compounds at about the same wavelength. The reflectance at long wavelengths is less for (ATTF)(TCNQ) than for (TTF)(TCNQ) while for (TMTTF)(TCNQ) it is somewhat greater. Since this portion of the spectrum depends mostly on the electron scattering time, we may conclude that the conductivity of (ATTF)(TCNQ) is slightly less than that of (TTF)(TCNQ), and that (TMTTF)(TCNQ) has a higher conductivity than (TTF)(TCNQ). This is discussed quantitatively below.

IV. TRANSVERSE DIELECTRIC FUNCTION FOR AN ANISOTROPIC METAL

The semiclassical (Drude) dielectric function $\epsilon(\omega)$ for a metal (ignoring interband transitions) is given by the expression,

$$\epsilon(\omega) = \epsilon_{\text{core}} - \frac{\omega_p^2}{\omega^2 + i\omega/\tau} \equiv \epsilon_1 + i\epsilon_2 , \tag{3}$$

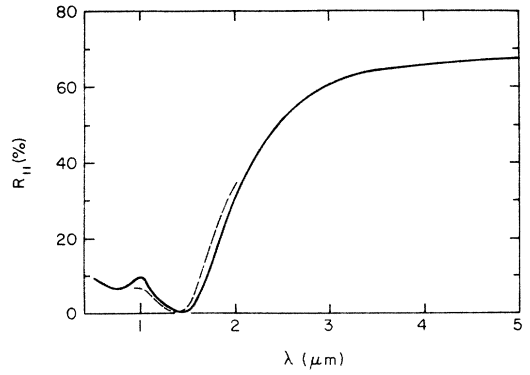

FIG. 5. Reflectance of (TTF) (TCNQ) for light polarized parallel to the conducting axis. Solid curve: spectrum derived from the data in Fig. 4; dashed curve: single-crystal spectrum.

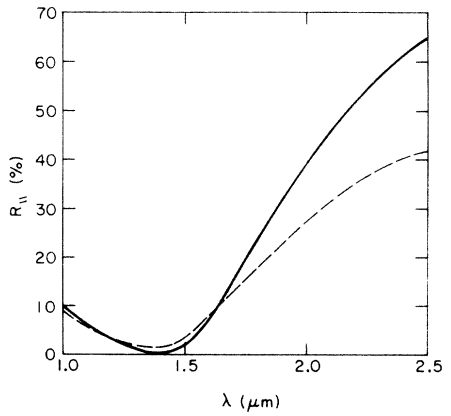

FIG. 6. Reflectance of (ATTF) (TCNQ) and (TMTTF) (TCNQ) for light polarized parallel to the conducting axis. The spectra are derived from polycrystalline measurements. Solid curve: (TMTTF) (TCNQ); dashed curve: (ATTF) (TCNQ).

where

$$\omega_p^2 = 4\pi N e^2/m^* , \tag{4}$$

ϵ_{core} is the residual dielectric constant at high frequency arising from core polarizability, τ is the electronic relaxation time, ω_p is the plasma frequency, N is the electron density, and m^* is the optical effective mass. In terms of the real and imaginary parts of ϵ, the reflectance is given by,

$$R = \frac{1 + |\epsilon| - [2(|\epsilon| + \epsilon_1)]^{1/2}}{1 + |\epsilon| + [2(|\epsilon| + \epsilon_1)]^{1/2}} , \tag{5}$$

where $|\epsilon| = (\epsilon_1^2 + \epsilon_2^2)^{1/2}$. Equation (3) implicitly assumes an isotropic free-electron gas. (TTF)(TCNQ) is however, highly anisotropic in its crystal structure[15] and electronic properties.[4-8] The effect of the implied anisotropic band structure on the dielectric function must be considered. The transverse dielectric function for the case of an anisotropic metal is[30]

$$\epsilon_{\perp}(\omega) = 1 - \frac{4\pi n e^2}{\omega^2} \left\langle \frac{\partial^2 \epsilon_0}{\partial k_z^2} \right\rangle + (\text{frequency-independent contribution from filled bands}), \tag{6}$$

where n is the electron density, $\epsilon_0(k)$ is the dispersion relation for electrons in the conduction band, and the electric field is applied in the z direction, which is assumed parallel to a symmetry axis of the crystal. This result is similar to Eq. (3) in the isotropic limit, using the conventional definition of the effective mass. One can phenomenologically generalize Eq. (6) to include the important lifetime and scattering effects by replacing ω^2 in the denominator with $\omega(\omega + i/\tau)$.

We see that for anisotropic materials the appro-

priate expression for the effective mass involves only derivatives with respect to the component of $\vec{k}$ along the electric field direction (provided the field is oriented along a symmetry axis of the crystal). Thus, the plasma frequency is similarly anisotropic.

V. DISCUSSION OF EXPERIMENTAL RESULTS

The reflectance data were fitted to Eq. (5), with $\epsilon(\omega)$ given by Eq. (3), over the wavelength range from 1.25 to 2.1 μm to determine values for ϵ_{core}, ω_p, and τ. A nonlinear least-squares computer routine was used.[31] The effect of a contribution to ϵ_2 related to the peak at 1 μm is unimportant for wavelengths greater than 1.2 μm (see discussion below). The best fit at room temperature was obtained with $\epsilon_{core}=2.43$, $\omega_p=1.80\times10^{15}$ sec^{-1} ($\hbar\omega_p=1.2$ eV), and $\tau=2.83\times10^{-15}$ sec. This fit ($\chi^2\sim10^{-4}$) represents average deviations of ~1% for each point, or within the experimental limits. The value of ϵ_{core} is consistent with expected core polarizability contributions for molecular crystals.

It should be noted that "metallic reflection" may occur in regions of imaginary refractive index near a strong electronic transition.[32] Such behavior (as suggested in Ref. 5) could be expected to produce a reflectance edge similar to that observed at 1.4 μm, if a sufficiently strong transition were present near this frequency. To check this possibility, the reflectance in Fig. 3 was fitted to a Lorentzian oscillator using the relation

$$\frac{\epsilon-1}{\epsilon+2}=\frac{\frac{1}{3}\omega_p^2}{\omega_0^2-\omega^2+i\Gamma\omega}+G\,, \tag{7}$$

where ω_0 is the resonance frequency, Γ is the relaxation rate, ω_p^2 is the plasma frequency squared and is related to the oscillator strength, and G is a constant contribution from other sources. This expression assumes cubic symmetry. It should,

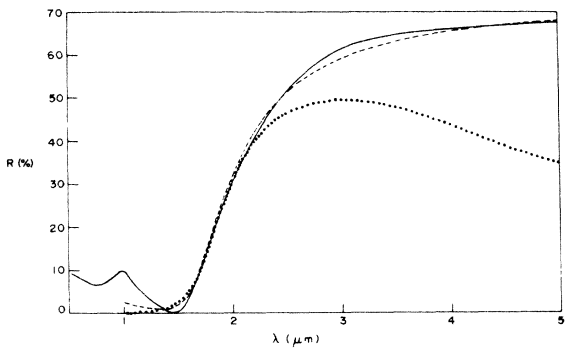

FIG. 7. Comparison of $R_{\|}$ derived from compaction measurements (solid curve) with least-squares fits to the data for two models. Dashed curve: Drude model; dotted curve: strong Lorentzian oscillator model. The fits were performed for $1.2\leq\lambda\leq2.1$ μm.

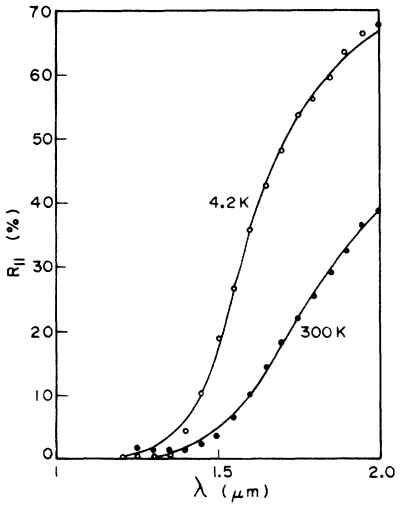

FIG. 8. Single-crystal reflectance of (TTF) (TCNQ) for light polarized parallel to the conducting axis at room temperature and at 4.2 K. The solid lines are the least-squares fits of the data points to Eq. (3). At 300 K, $\epsilon_{core}=2.40$, $\omega_p=1.79\times10^{15}$ sec^{-1}, $\tau=3.1\times10^{-15}$ sec. At 4.2 K, $\epsilon_{core}=2.15$, $\omega_p=1.80\times10^{15}$ sec^{-1}, $\tau=6.1\times10^{-15}$ sec.

however, give a reasonable qualitative estimate for the local fields in a noncubic system as well. The best fit between 1.2 and 2.1 μm was obtained with $\omega_0=0.79\times10^{15}$ sec^{-1}, $\omega_p=1.0\times10^{15}$ sec^{-1}, $G=0.073$, and $\Gamma=0.25\times10^{15}$ sec^{-1}. The calculated reflectance decreased steadily at wavelengths beyond 2.5 μm, however, in contrast with the experimental results. In Fig. 7, the reflectance spectrum derived from the compaction data is compared with the best fits from both the Drude formula [Eq. (3)] and the Lorentzian oscillator [Eq. (7)]. The Drude fit agrees well with the experimental curve at all wavelengths up to 5 μm, while the Lorentzian fit begins to fail beyond 2 μm. Moreover, absorption measurements on polycrystalline thin films of (TTF)(TCNQ) show no evidence of the strong, sharp absorption near 2.4 μm implied by the fit values of ω_0 and Γ above.[29,33] The experimental evidence, then, strongly favors the interpretation of the observed edge at 1.4 μm as a plasma edge described by Eq. (3).

Polarized single-crystal reflectance spectra were measured from 1.2 to 2.0 μm at several discrete temperatures from 300 to 4.2 K. The results were analyzed in the same way as for the room-temperature data to find the optimum values of parameters ϵ_{core}, ω_p, and τ. The reflectance data and the least-squares fits are shown in Fig. 8 for one sample at 300 and 4.2 K. The least-squares values of ϵ_{core}, ω_p, and τ for several samples at several temperatures are given in Table I. Note that the plasma frequency does not change throughout this temperature range. In particular,

TABLE I. Summary of data obtained from least-square Drude fits to single-crystal data. Successive runs on a given sample were made after cycling to low temperature.

Sample	Run	Temperature (K)	ϵ_{core}	ω_p (10^{15} sec^{-1})	τ (10^{-15} sec)
c	*c*-1	300	2.40	1.79	3.1
c	*c*-3	300	2.48	1.80	2.5
a	*a*-1	300	2.50	1.80	3.4
a	*a*-2	300	2.43	1.79	2.8
b	*b*-1	286	2.47	1.79	2.6
b	*b*-1	255	2.47	1.79	2.6
c	*c*-3	207	2.39	1.79	2.3
c	*c*-2	186	2.36	1.80	3.0
c	*c*-3	148	2.21	1.80	2.8
c	*c*-1	70	2.15	1.80	6.0
c	*c*-1	35	2.15	1.80	6.1
c	*c*-1	4.2	2.15	1.80	6.1
c	*c*-3	4.2	2.12	1.79	3.5

there is no change in ω_p below the transition temperature. From this fact it can be concluded that the magnitude of the energy gap in the low-temperature phase is much less than the photon energies in the optical experiments, i.e., $\omega_g \ll \omega_p$. This is consistent with all other results regarding the energy gap in (TTF)(TCNQ).[1,2,8,11,13] In addition, the lack of change in ω_p rules out many possible mechanisms for the metal-insulator transition. For example, it has been suggested[2,7] that either double charge transfer or back transfer to the neutral molecules would lead to filled bands and an insulating ground state. Both of these models imply that the conduction-electron density vanishes at low temperatures. The lack of any temperature dependence to the plasma frequency demonstrates conclusively that no such change in the electron density occurs. Thus there is strong evidence in favor of the interpretation of the phase transition as being due to a small energy gap opening up at the Fermi surface without a major change in the number density of electrons and holes.

The magnitude and temperature dependence of ω_p and ϵ_{core} as reported by Grant *et al.*[5] differ from the results in Table I. We speculate that this difference arises because of differences in the spectral range over which the fits were performed. In particular, extending the fit to shorter wavelengths, where interband contributions to the reflectance become important, would overestimate the value for ϵ_{core}. In addition, since the reflectance minimum is located at $\omega_p/\epsilon_{core}^{1/2}$, a larger value of ω_p would result as well. We note that the values of $\omega_p/\epsilon_{core}^{1/2}$ calculated from Ref. 5 agree well with the values obtained from Table I; i.e., $\omega_p/\epsilon_{core}^{1/2} \approx 0.80 \pm 0.04$ eV. The variation with temperature of this quantity is ~5%, or comparable to the uncertainty in ϵ_{core}.

The peak at 1 μm in Figs. 3 and 5 for polarization parallel to the conducting axis was attributed[4] to the onset of the interband transitions responsible for the strong parallel absorption in the visible region of the spectrum. The implied value of ϵ_2 at the peak resulting from this assignment is consistent in magnitude with the optical density as observed in the visible transmission experiments. Setting the skin depth $\delta = 1/\alpha \lesssim 3\times10^{-5}$ cm, the relation

$$\delta = (c^2/2\pi\sigma\omega)^{1/2} \tag{8}$$

gives a conductivity $\sigma \gtrsim 10^{14}$ at $\omega = 1.8\times10^{15}$ sec^{-1}. The resulting value of $\epsilon_2 = 4\pi\sigma/\omega \gtrsim 0.5$ produces an increase in the reflectance of the observed magnitude. As may be verified from the analysis above, the Drude contribution to ϵ_2 from Eq. (3) is $\epsilon_2 \simeq 1/\omega\tau \simeq 0.16$. Thus the interband contribution should dominate at and above this frequency, resulting in an increased reflectivity. The Drude fits do consistently fall below the experimental data at wavelengths shorter than 1.2 μm as shown in Figs. 7 and 8.

Several interesting properties of (TTF)(TCNQ) may be calculated from the experimental data. The conventional expression relating the plasma frequency and the dc conductivity for a metal is

$$\sigma = \omega_p^2 \tau/4\pi . \tag{9}$$

Using the above values for ω_p and τ, one obtains an estimate of 10^3 $(\Omega\,\mathrm{cm})^{-1}$ for the conductivity along the *b* axis in good agreement with the measured dc value at room temperature.[1]

The effective mass m^* can be found from Eq. (4). Using the value of $N = 4.7\times10^{21}/\mathrm{cm}^3$ calculated from the x-ray data[15] assuming complete charge transfer, m^* is found to be $5m_e$, where m_e is the free-electron mass. The optical effective mass may, in turn, be used to estimate the bandwidth. The electrical conductivity for a nearly-half-filled one-dimensional tight-binding band is given by[14]

$$\sigma = \frac{4N}{\pi}\frac{e^2\tau\, ta^2}{\hbar^2} , \tag{10}$$

where t is the tight-binding transfer integral, and a is the lattice constant. Comparing Eqs. (9) and (10), the effective mass is seen to be

$$m^* = \pi\hbar^2/4ta^2 . \tag{11}$$

It is easily seen that this expression agrees with the conventional definition,

$$\frac{1}{m^*} = \frac{1}{\hbar^2}\left\langle\frac{\partial^2\epsilon_k}{\partial k^2}\right\rangle \tag{12}$$

averaged over the occupied states of the half-filled tight-binding band. Writing the energy as

$$\epsilon_k = -2t\cos ka , \tag{13}$$

we have

$$\frac{\partial^2\epsilon_k}{\partial k^2} = 2ta^2\cos ka \tag{14}$$

and

$$\frac{1}{m^*} = \frac{2ta^2}{\hbar^2} \frac{\int_0^{k_F} \cos ka\, dk}{\int_0^{k_F} dk} = \frac{2ta^2}{\pi\hbar^2} \frac{\sin k_F a}{k_F a} \tag{15}$$

in agreement with Eq. (11) for $k_F = \pi/2a$. This result is strictly valid only in the tight-binding limit. Deviations from this limit are expected to lead to differences between the optical and band effective masses. In addition, less than complete charge transfer would lead to a smaller effective mass and a larger transfer integral. Using the experimental value, $m^* = 5m_e$ as obtained from ω_p for the half-filled band, leads to a value for t of 0.1 eV. This is in agreement with the values of about 0.1 eV determined from the room-temperature-susceptibility experiments[11] and from the thermoelectric-power data.[10]

The electronic structure of (TTF)(TCNQ) involves two electronic subsystems on the TTF and TCNQ chains, respectively. In this case, there would be no reason to expect equal electron densities or effective masses on the two chains. It is clear from Eq. (6) that the effective mass entering into the expression for the plasma frequency then represents a weighted average of the effective masses on the two chains. Labeling the chains 1 and 2, a trivial extension of Eq. (6) leads to the result

$$\omega_p^2 = 4\pi e^2 (n_1/m_1^* + n_2/m_2^*). \tag{16}$$

In such a two-chain model, it is this average effective mass which is derived from the plasma frequency observed in the reflectance.

The static dielectric constant at temperatures well below the transition temperature can be calculated assuming a one-dimensional small-band-gap semiconductor model. The result is given by[8,34,35]

$$\epsilon_1^b(0) = 1 + 0.65\,(\omega_p/\omega_g)^2, \tag{17}$$

where $\hbar\omega_g = E_g$ is the minimum (direct) energy gap. Using the measured value of the plasma frequency with $\hbar\omega_g/k_B = 150 \pm 30$ K as determined by conductivity,[2] susceptibility,[11] and nuclear-relaxation[13] measurements, the dielectric constant is predicted to be 4000, in good agreement with the value obtained by microwave measurements in this laboratory ($\epsilon_1^b \simeq 3200$).[8]

The least-squares fits to the room-temperature reflectance spectra of (ATTF)(TCNQ) and (TMTTF)(TCNQ)(Fig. 6) lead to the values $\epsilon_{core} = 2.4$, $\omega_p = 1.78\times10^{15}$ sec^{-1} and $\tau = 2.2\times10^{-15}$ sec for the former, and $\epsilon_{core} = 2.8$, $\omega_p = 1.83\times10^{15}$ sec^{-1} and $\tau = 4.3\times10^{-15}$ sec for the latter. These values are similar to the results for (TTF)(TCNQ). The room-temperature optical conductivity of (ATTF)(TCNQ) is, from Eq. (8), 600 $(\Omega\,\mathrm{cm})^{-1}$, and the conductivity of (TMTTF)(TCNQ) is 1300 $(\Omega\,\mathrm{cm})^{-1}$.

VI. ELECTRON SCATTERING TIME

Examining Table I, it is seen that ω_p does not change over the entire temperature range, while ϵ_{core} changes only slightly. The values of τ increase as the temperature decreases, but the values do not reproduce from run to run, even for a single sample. It was found that the measured value of τ for a particular sample invariably decreased (see Table I) after repeated temperature cycling, indicating an extreme sensitivity to strains and defects induced by differential thermal contractions relative to the copper mounting plate. This defect sensitivity is expected for a pseudo-one-dimensional system with large anisotropy, since individual chain breaks would have a drastic effect.[1,3,6] Consequently, to obtain a meaningful temperature dependence requires acquisition of a full set of data on each temperature run. It may be noted in Fig. 8 that the reflectance at 2 μm is very sensitive to the value of τ (recalling that ω_p and ϵ_{core} do not vary appreciably). Thus by measuring the reflectance at this wavelength as the temperature is varied, the temperature dependence of τ may be monitored continuously. The results of this procedure for several samples are shown in Fig. 9, where $1/\tau$ is presented as a function of temperature. Also shown are the discrete temperature results for the first run on a single sample. The agreement between the two measurement techniques is seen to be good. It may be noted that at high temperatures ($T \gtrsim 100$ K) the relaxation time varies inversely with temperature, while at low temperatures τ saturates and approaches a constant value.

For some samples it was noted that as the temperature decreased, $1/\tau$ increased abruptly and then resumed its gradual decrease. This behavior is interpreted as being caused by defects induced by strains, as noted above. Such defects would add a temperature-independent contribution to $1/\tau$ (i.e., residual resistivity), consistent with the observed behavior. The abrupt changes in the measured values of τ could also be explained by movement of the sample, causing a drop in the signal level due to misalignment. This possibility was eliminated by checking sample alignment at 4.2 K. No change was observed in the sample orientation, indicating that movement of the sample was not involved. In addition, it may be noted that these changes invariably occurred well below room temperature, where the vacuum grease holding the samples in place had solidified. This not only immobilized the sample but also caused the buildup of strains.

The absolute accuracy of the measured values of $1/\tau$ is about 10%. However, as indicated by the error bars in Fig. 9, the relative error is much

smaller, around 3%. Most of the error results from uncertainty in the absolute calibration of the reflectance due to differences in the effective areas of the sample and the reference mirror and differences in the alignment. This error affects all the measurements in the same way, however, and results in little change in the qualitative features of the temperature dependence of $1/\tau$. The major effect is a slight vertical shift of the curve, changing the apparent value of the temperature-independent contribution. The relative values of τ may be affected by use of an incorrect value for ϵ_{core}. Variations in ϵ_{core} over the range represented in Table I lead to a relative error within the 3% limit quoted.

The single-crystal reflectance measurements on (TTF)(TCNQ) reported by Grant *et al.*[5] are in close agreement with those reported in our first paper[4] and presented more completely here. However, the scattering time reported[5] is considerably shorter than that obtained from our data (see Fig. 9). The temperature dependence appears to be somewhat weaker, although the large scatter implies large error bars. Evidently, in their samples, the scattering time is limited by a large temperature-independent contribution from defects and impurities, i.e., residual resistivity, which increases the total scattering rate. This is consistent with our more thorough temperature-cycling studies which clearly demonstrate the increased residual defect resistivity.

The relaxation time τ and its temperature dependence provide a valuable probe for investigating the electron-phonon interaction. Assuming the electron-phonon Hamiltonian to be of the conventional form

$$H_{ep} = \sum_{k,q} g(q)\, c^{\dagger}_{k-q}\, c_k\, (b^{\dagger}_q + b_{-q}) \tag{18}$$

(where the $c^{\dagger}$ are the electron creation operators, the $b^{\dagger}$ are the phonon creation operators) the total scattering rate appropriate to optical processes is derived in Appendix A and given in Eq. (A6). The result is

$$1/\tau = (2\pi/\hbar)\,\lambda\,(k_B T + \tfrac{1}{2} k_B \Theta_D) \tag{19}$$

where λ is the dimensionless electron-phonon coupling constant. Thus, at high temperatures ($T > \Theta_D$), τ^{-1} is proportional to the number of thermal phonons and thus to the temperature. As first pointed out by Holstein,[36] at low temperatures ($T < \Theta_D$), τ^{-1} saturates because of phonon emission to a value given by

$$1/\tau_{\text{em}} = (2\pi/\hbar)\,\lambda\,\tfrac{1}{2} k_B \Theta_D\,, \tag{20}$$

so that measurement of τ^{-1}_{em} and Θ_D lead directly to a value for λ through Eq. (20), whereas the determination of $d\tau^{-1}(T)/dT$ yields an independent value through Eq. (19).

The comparison of the room-temperature experimental results [Eq. (8)] with the dc conductivity supports the conclusion that the scattering is dominated by phonons. The linear temperature dependence of $1/\tau$ as shown in Fig. 9 at temperatures above $\Theta_D = 89$ K[37] is additional strong evidence in support of this conclusion. Note that in addition to the phonon emission effect noted above, defect or impurity scattering also leads to a saturation of τ as described above in the cycling experiments. Since phonon emission does not contribute to the scattering at frequencies below the phonon frequencies, we should subtract this contribution from the optical scattering rate before making any comparison with the dc resistivity. Using Eq. (19), we find

$$\frac{1}{\tau_{\text{em}}} = \frac{1}{2}\,\frac{d[\tau^{-1}(T)]}{dT}\,\Theta_D\,, \tag{21}$$

so that $1/\tau_{\text{em}} \simeq 5\times 10^{13}$ sec^{-1}. The inclusion of coupling to the various optical phonons as well as the hindered molecular rotations might lead to a somewhat larger saturation value,[4] although the above value is in agreement with the extrapolated value obtained from the best data (largest τ) on Fig. 9. When the phonon emission contribution is subtracted

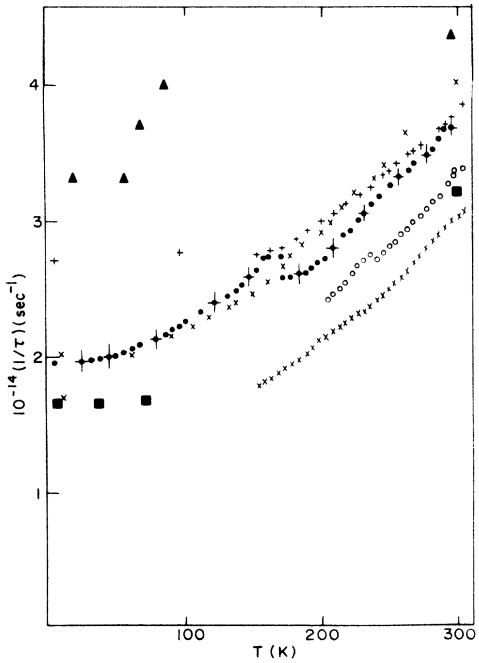

FIG. 9. Reciprocal of the scattering time as a function of temperature for several samples. The breaks in some of the curves are caused by strain-induced defects in the samples as described in the text. ■, data from Table I (least-squares fits to single-crystal data); ▲, data from Ref. 5; ×, two runs on a given sample showing the residual resistivity effect. The other symbols represent different samples.

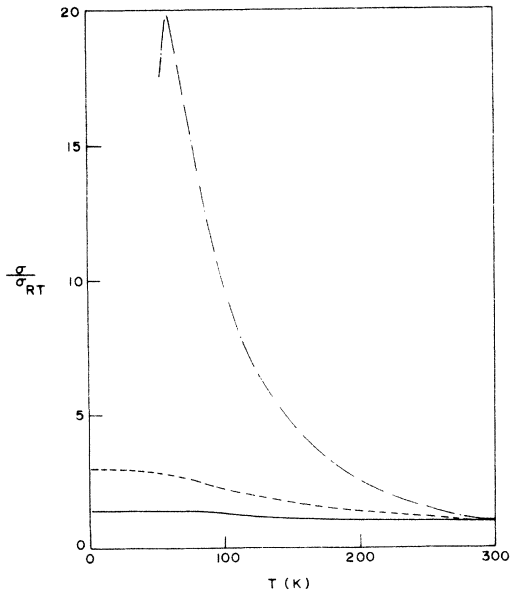

FIG. 10. Normalized conductivity of (TTF) (TCNQ). Dot-dash curve, typical dc single-crystal data. Dashed curve, single-particle conductivity as obtained from ir reflectivity with $\tau_{def}^{-1} = 1\times10^{14}$ sec^{-1}. Solid curve, single-particle conductivity as obtained from ir reflectivity with $\tau_{def}^{-1} = 2.8\times10^{14}$ sec^{-1}.

from the $1/\tau$ curve, the defect contribution is seen to be small compared to the phonon scattering contribution at high temperatures in the best samples, but does contribute significantly in poorer quality samples especially after multiple temperature cycling. From Fig. 9 we see that $1/\tau_{def} \gtrsim 1\times10^{14}$ sec^{-1}. Equation (9) or (10) then gives $\sigma_{def} \lesssim 3000$ $(\Omega\,\mathrm{cm})^{-1}$. This value represents the maximum conductivity due to single-particle processes. The peak value of the dc conductivity, however, is several times higher than this value, even for crystals showing typical behavior with $\sigma_{max}/\sigma_{RT} \simeq 15$–$20$. This result strongly implies that there is excess dc conductivity associated with a many-body collective effect in all (TTF)(TCNQ) crystals.

Also shown on Fig. 9 are the scattering rates obtained from infrared-reflectivity studies of samples prepared by Grant *et al.*[5] Of particular interest is the result that $\tau \simeq 2.3\times10^{-15}$ sec, roughly a factor of 1.5 shorter than the room-temperature value obtained from our best samples. Comparing these data with those reported here, and noting the sensitivity to temperature cycling with the associated growth of a temperature-independent contribution, leads to the conclusion that the Grant *et al.* samples are highly defected either by impurities or chain perturbations such that the residual resistivity is given by

$$\rho_0 = (\omega_p^2 \tau_0/4\pi)^{-1} = 1.5\times10^{-3}\ \Omega\,\mathrm{cm}\,. \qquad (22)$$

Since this value is comparable to the typical room-temperature values obtained at dc, one expects to observe essentially no temperature dependence in the normalized conductivity obtained from such samples. On the contrary, conductivity studies on such crystals demonstrate $\sigma_{max}/\sigma_{RT} \simeq 16$,[38] and higher values have been observed.[39] The point is clear. It appears that the measured dc resistivity regularly falls *below* the measured residual resistivity (from single-particle scattering off defects and/or impurities) by more than an order of magnitude, implying that the dc conductivity is carried in a collective manner.

This is shown schematically in Fig. 10, where we plot the normalized dc conductivity for a typical crystal of (TTF)(TCNQ) with $\sigma_{max}/\sigma_{RT} \simeq 20$. For comparison we plot the single-particle contribution as inferred from the temperature dependence of the optical data. The dashed curve assumes $1/\tau_{def} = 1\times10^{14}$ sec^{-1} as obtained from the longest τ data of Fig. 9. The solid curve assumes $1/\tau_{def} = 2.8\times10^{14}$ sec^{-1} as obtained from the data of Ref. 5. The temperature dependence of the dc data is steeper, and the maximum exceeds the "residual resistivity" value by a large factor.

VII. OPTICAL PROPERTIES OF A ONE-DIMENSIONAL NARROW-BAND METAL: FREQUENCY DEPENDENCE OF τ

Implicit in the above argument is the assumption that the optically measured τ corresponds to the scattering of electrons near the Fermi surface. We examine the validity of this assumption by considering the processes of optical absorption in a one-dimensional narrow-band conductor.

In a three-dimensional free-electron gas, the elementary excitations consist of a broad continuum of single-particle excitations of energy $\epsilon_q = \epsilon_{k+q} - \epsilon_k$. In addition there is a branch of collective modes, or plasma oscillations, which occur at low-q values. For large q, the plasmon branch merges with the single-particle excitation band, and the plasma modes cannot exist because of decay into the single-particle excitations of equal energy and momentum. The lifetime of $q = 0$ plasmons is limited by emission of an electron-hole pair (single-particle excitation) with approximately the same energy and a single phonon to conserve momentum.

In a one-dimensional tight-binding metal there are significant modifications to this result. Considering the tight binding band in Fig. 11(a), it is clear that zero-energy excitations are possible only at $q = 0$ and $q = 2k_F$. At $q = 2k_F$, all excitation energies from $\epsilon_q = 0$ to $2E_F$ are possible, but at smaller-q values a more limited range of ϵ_q values is permitted. We are led to a single-particle excitation spectrum shown in Fig. 11(b). Note that

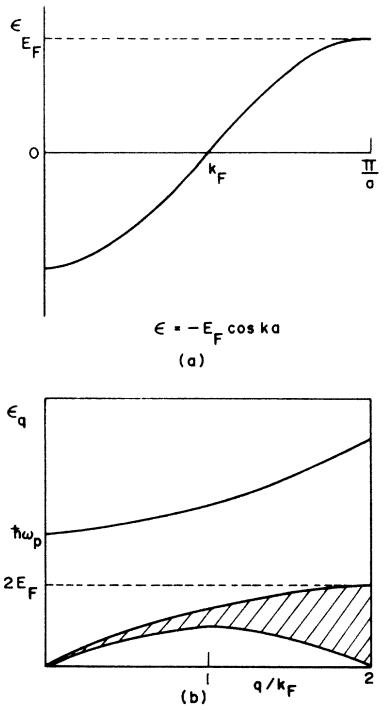

FIG. 11. (a) One-dimensional half-filled tight-binding band; (b) elementary excitations for the tight-binding band.

in a highly anisotropic but not strictly one-dimensional system, additional low-energy excitations are possible. As the anisotropy decreases, the "hole" in the excitation spectrum in Fig. 11(b) is gradually filled in.

The important difference between the free-electron and the one-dimensional narrow band cases is that, in the latter, no single-particle excitations are allowed at energies greater than $2E_F$. If, as is likely to be the case in organic molecular crystals, the plasma frequency is higher than $2E_F/\hbar$, the plasma modes need not be cut off at large q values by the single-particle excitations. We must examine the effect this has on the reflectivity. Since there may not be single-particle excitations degenerate with the plasmon energy, plasmon decay cannot occur by the emission of a single electron-hole pair and a phonon as envisioned in the Drude theory, and higher-order scattering processes are required. In this case the implicit assumption of a frequency independent scattering time in Eq. (3) breaks down. Thus the scattering time deduced from Eq. (3) at frequencies near ω_p may in general be unrelated to the scattering time in the dc conductivity. The use of Eqs. (2) and (19) to calculate the electron-phonon interaction parameter would in this case not be valid.

A possible resolution of this problem comes about if interband transitions of appropriate energies are present. In particular, consider the band structure shown in Fig. 12(a). It is easily seen that the interband transitions lead to the single-particle excitations shown in Fig. 12(b). If $E_1 > \hbar\omega_p > E_2$, the plasmon branch will be as shown. The scattering time measured optically might then be expected to be consistent with the dc conductivity value, since the plasmons can decay by the conventional single-phonon process.

An alternate approach to the question may be instructive. We consider the Drude absorption by looking at the phonon-assisted intraband and interband absorption of photons. In lowest-order perturbation theory there are two independent processes with initial state k^0 and final state $(k+q)^n$, where the superscript is the band index (see Fig. 13). In the first, the electron is scattered by a phonon into the state $(k+q)^0$ and then absorbs a photon of energy, $\hbar\omega$, resulting in a final state $(k+q)^n$. In the second process, the electron first absorbs the photon and then scatters from a phonon. This process is forbidden in the free-electron model, since there is no intermediate state k^n at $q=0$. Note that the first process involves initial-state electron-phonon scattering and thus measures τ in the vicinity of the Fermi energy. Electrons deep below E_F cannot be involved because the scattered intermediate state would be

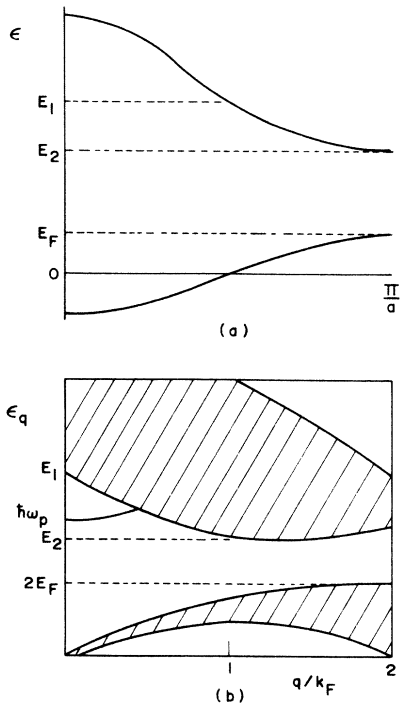

FIG. 12. (a) One-dimensional tight-binding band structure with more than one band; (b) elementary excitations for tight-binding bands with interband transitions included.

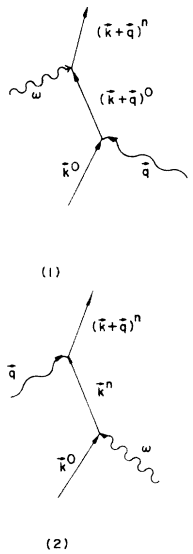

FIG. 13. Phonon-assisted absorption of photons: (1) electron is scattered by a phonon and then absorbs a photon; (2) electron absorbs a photon and then scatters from a phonon.

full, while states well above E_F are not occupied. This process, then, would be expected to measure the scattering time characteristic of electrons within roughly kT of E_F and thus the τ corresponding to the conductivity.

The second process involves final-state electron-phonon scattering. The scattering time here need not in general bear any relation to the τ in the conductivity. However, since it is a single-phonon process, it will have the same temperature dependence. Note that the initial and final states are indistinguishable, so one must add the matrix elements and subsequently square the sum to get the total transition rate. The matrix element for the first process may be written

$$M_1 = \sum_q \frac{\langle (k+q)^n | H_{\text{E-M}} | (k+q)^0 \rangle \langle (k+q)^0 | H_{\text{ep}} | k^0 \rangle}{\epsilon_0(k+q) - \epsilon_0(k) \pm \hbar\omega_q} , \tag{23}$$

where H_{ep} is the electron-phonon term in the Hamiltonian, $H_{\text{E-M}}$ represents the coupling to the electromagnetic field, and $\hbar\omega_q$ is the phonon energy. For the second process, we have

$$M_2 = \sum_{k^n} \frac{\langle (k+q)^n | H_{\text{ep}} | k^n \rangle \langle k^n | H_{\text{E-M}} | k^0 \rangle}{\epsilon_n(k) - \epsilon_0(k) - \hbar\omega} . \tag{24}$$

Comparing M_1 and M_2 we see that the energy denominator for M_2 is large if $\hbar\omega$ is well below the interband transitions at $q = 0$. On the other hand, the denominator in M_1 may be very small or even zero (the apparent divergence in Eq. (23) is removed by inclusion of the term for the exchange process). Thus, in this case we expect $M_1 \gg M_2$. As ω approaches the interband transitions, the contribution from the second process is expected to increase, leading to a decrease in the measured scattering time. This effect is observed experimentally in nearly-free-electron metals such as gold, aluminum, and silver.[40]

We see from this discussion that the optical absorption, and hence the reflectance also, at frequencies sufficiently far below the $q = 0$ interband absorption edge is dominated by the scattering of electrons near the Fermi surface. From the above discussion we can then conclude that the scattering time measured in reflectance experiments at these frequencies is expected to correspond to the scattering time in the dc conductivity.

The question ultimately must be answered experimentally. The following criteria may be appropriate: (a) there is evidence that Fig. 12 correctly describes the excitation spectrum; (b) the reflectance can be fitted adequately with a frequency independent τ over a wide frequency range; (c) the resulting value of τ is consistent with the dc conductivity; (d) the temperature dependence of the optically measured scattering time is consistent with expectations based on single-phonon processes; (e) there is evidence of appreciable absorption throughout the frequency range of interest. If these conditions are satisfied, the above model may be considered adequate.

We have seen that the reflectance may be fitted to an expression involving a frequency independent τ over a wide frequency range. The value of τ is consistent in magnitude with the dc conductivity, and its temperature dependence suggests that τ is dominated by single-phonon scattering. There is evidence that interband transitions are present at energies somewhat higher than ω_p. In addition, there is direct evidence of Drude absorption [i.e., $\sigma_1(\omega)$ has the frequency dependence predicted by Drude theory] throughout the infrared,[29] suggesting the existence of final states at all photon energies in this range in Eqs. (23) and (24). We may, moreover, estimate the ratio M_1/M_2 by letting the denominator in Eq. (24) take the minimum possible value, i.e., $E_{\text{interband}} - \hbar\omega_p \simeq 0.4$ eV. The denominator in Eq. (23), on the other hand, is on the order of a phonon energy, or about 0.01 eV. Thus $M_1 \gg M_2$, so we see that the scattering time at these frequencies should be dominated by scattering of electrons near the Fermi surface, and the use of a frequency-independent scattering time is well justified.

VII. SUMMARY AND CONCLUSIONS

In this paper we have investigated the optical properties of (TTF)(TCNQ) in the visible and near infrared. We have analyzed the experimental results in terms of simple Drude theory, with cor-

rections made for anisotropic effects introduced by the anisotropic band structure. The inclusion of a frequency dependence in the electron scattering time was found to be unnecessary. The reflectance spectrum for polarization parallel to the conducting axis showed a plasma edge at about 1.4 μm. The plasma frequency was used to infer a value for the effective mass and the tight-binding transfer integral. The plasma frequency and the scattering time led to a conductivity consistent with the measured room-temperature dc value. All of this information confirms that at room temperature, (TTF)(TCNQ) is a highly anisotropic (pseudo-one-dimensional) metal.

Studies of the related materials (ATTF)(TCNQ) and (TMTTF)(TCNQ) showed a similar behavior. Thus it may be concluded that the addition of small amounts of disorder or the slight modification of the molecular structure of TTF has a minimal effect on the optical properties of the salt. The electronic structure was seen to include a tight-binding conduction band with a transfer integral $t \simeq 0.1$ eV, and higher energy bands causing optical absorptions beginning 1.2 eV above the Fermi level. At low temperatures the plasma frequency was used to calculate the static dielectric constant. The good agreement with experiment[8] indirectly supports the measured value of the energy gap.[2,11,13]

The temperature dependence of the scattering time was found to be consistent with single-phonon scattering, with a contribution from defect scattering which varies from sample to sample and which increases as the number of defects increases. The possibility exists, of course, that some mechanism other than the electron-phonon interaction could be responsible for the scattering. For example, it is conceivable that electrons on one type of chain could couple via the Coulomb interaction to thermally excited charge density waves on the neighboring chains of the other type. The experimental evidence, however, suggests that the electron-phonon interaction is involved. The low-temperature x-ray data show a broadening of the x-ray linewidth as the temperature decreases toward the transition temperature.[41] Thus fluctuations in the lattice become large in the vicinity of the electronic phase transition, suggesting the importance of electron-phonon coupling. In addition, the thermal expansion coefficient is unusually large.[42] This implies a strong anharmonicity in the lattice modes, suggestive again of strong coupling to the electronic system. Recent measurements of the elastic moduli[43] confirm this interpretation.

Experimental considerations aside, we may expect a large electron-phonon coupling in systems such as (TTF)(TCNQ). There are two important sources of electron-phonon coupling[3]: phonon modulation of the intermolecular electron transfer integral and phonon modulation of the solid-state ionization potential. The transfer integral scales with the overlap integral and is, therefore, expected to vary exponentially with distance between molecules. The solid-state ionization potential is affected by the electrostatic Madelung energy and the polaron polarization bond energy. Since the polaron energy is a strong function of distance, r^{-4}, the ionization potential is also expected to be sensitive to lattice vibrations. Thus both sources of electron-phonon coupling are expected to contribute, and the conclusion that the experimentally observed mean free path and scattering time result from phonon scattering is reasonable. As an estimate we note that the Madelung and polarization energies must be of order 1 eV to assure charge transfer and the stability of the salt. Consequently, one expects an electron-phonon coupling constant $\gamma \sim 1$ eV per lattice constant, or $\gamma \sim 2\times10^7$ eV/cm.

As noted in Sec. I, the dimensionless electron-phonon interaction parameter λ may be obtained from the infrared studies. Using Eqs. (2) and (19), and the linear contribution to $1/\tau$ as shown in Fig. 9, one finds the strong coupling value of $\lambda \simeq 1.3$. An independent value can be obtained from Eq. (20) which relates the saturation value (phonon emission) to λ and the Debye temperature. The saturation value can be obtained from extrapolating the linear dependence of the largest τ data in Fig. 9, giving $1/\tau_{em} \simeq 5\times10^{13}$ sec^{-1}. This value, together with $\Theta_D \simeq 89$ K, also leads to $\lambda \simeq 1.3$.

Writing $\lambda = (\gamma^2/K)(1/2\pi t)$,[44] where K is the force constant ($\hbar\omega_D = 2\sqrt{K/M}$; ω_D is the Debye frequency and M is the ion mass), and $(1/2\pi t)$ is the density of states at the Fermi level in a one-dimensional tight-binding band, we find $\gamma \simeq 4\times10^7$ eV/cm, in agreement with expectations based on the above considerations of the sources of electron-phonon coupling.

Note that, given λ and E_F, the Peierls-Fröhlich transition temperature can be estimated directly. In tight-binding theory, the transition temperature is given by[19,45,46]

$$k_B T_p = (4\gamma E_F/\pi e)\, e^{-1/\lambda} = 0.84\, E_F\, e^{-1/\lambda}, \qquad (25)$$

where $\gamma = 1.7811$ is an Euler constant. Using $E_F/k_B \approx 3000$ K, T_p is found to be about 10^3 K. This intriguing result suggests the possibility of a dynamic distortion on either the cation or anion chains similar to that found recently in studies of mixed valence Pt salts. The suggestion of Lee, Rice, and Anderson[47] that a mechanism involving such a transition temperature could explain the temperature dependence of the susceptibility is particularly interesting in this light. Diffuse x-ray and inelastic-neutron-scattering experiments on (TTF)(TCNQ) would clearly be of interest.

The comparison of the optical and dc conductivities shows that the dc conductivity at all temperatures above the transition temperature is *not* dominated by single-particle scattering, that there is *excess* dc conductivity, and that the steep temperature dependence of the conductivity in all (TTF)(TCNQ) crystals arises not from single-particle scattering but from a collective many-body effect. The strong coupling value of 1.3 found for the electron-phonon coupling constant suggests that the electron-phonon interaction will play a major role in the explanation of these phenomena.

ACKNOWLEDGMENTS

We thank Professor R. Hochstrasser for the loan of the microscope and auxiliary equipment used in the microspectrophotometer. Dr. R. Soulen was most helpful in arranging the gift of the DK-2 spectrometer from the Pennwalt Corp. We are grateful to Professor P. Soven for guiding us through the analysis of the dielectric function for an anisotropic metal. Several discussions with Professor J. R. Schrieffer are gratefully acknowledged. One of us (A.F.G.) acknowledges a DuPont Young Faculty Grant.

APPENDIX A: CALCULATION OF τ^{-1} DUE TO PHONON ABSORPTION AND EMISSION

We calculate in this appendix the effective residual scattering time τ_{eff} due to phonon emission at low temperatures. Using the golden rule, we write the total scattering rate as

$$1/\tau = (2\pi/\hbar)\,|\langle k-q, n_q \pm 1 | H_{\text{ep}} | k, n_q\rangle|^2 \times \delta(\epsilon_k - \epsilon_F)\,. \tag{A1}$$

The phonon energy does not explicitly appear, since for the optical processes in question, the energy conservation is achieved with the incident photons. The electron-phonon interaction H_{ep} is given by

$$H_{\text{ep}} = \sum_{k,q} g_q\, c^{\dagger}_{k-q}\, c_k\, (b^{\dagger}_q + b_{-q})\,. \tag{A2}$$

Here k and q represent the electron and phonon wave numbers, respectively, n is the phonon occupation number, ϵ_k is the electron energy in state k, ϵ_F is the Fermi energy, g_q is the electron-phonon coupling constant, and $c^{\dagger}_k$ and $b^{\dagger}_q$ are creation operators for electrons and phonons, respectively.

Separating the wave functions into electronic and phononic parts, the matrix elements are readily calculated for back scattering across the Fermi surface, $k_F \to -k_F$. Equation (A1) becomes

$$\frac{1}{\tau} = \frac{2\pi}{\hbar}\sum_q g_q^2\,(2\langle n_q\rangle + 1)\,N(\epsilon_F)\,, \tag{A3}$$

where the sum over k has been performed and $N(\epsilon_F)$ is the density of states at the Fermi surface. The term $\langle n_q\rangle$ gives the temperature-dependent term of the scattering rate, while the 1 represents the scattering due to spontaneous phonon emission. In a one-dimensional system such as (TTF)(TCNQ), the only important phonon is $q = 2k_F$. We then have

$$1/\tau = (2\pi/\hbar)\, g^2_{2k_F}\,(2\langle n_{2k_F}\rangle + 1)\,N(\epsilon_F). \tag{A4}$$

At temperatures $T \gg \Theta_D$, we may write

$$\langle n_{2k_F}\rangle = kT/\hbar\omega_{2k_F}\,. \tag{A5}$$

Using the definitions

$$\frac{2g^2}{\hbar\omega}\Big|_{2k_F} = \lambda \quad \text{and} \quad \hbar\omega_{2k_F} = k_B\Theta_D \tag{A6a}$$

we obtain

$$1/\tau = (2\pi/\hbar)\,\lambda\,(kT + \tfrac{1}{2}k_B\Theta_D) \tag{A6b}$$

where λ is the dimensionless electron-phonon interaction parameter [$\lambda = N(\epsilon_F)\,V$]. Writing

$$1/\tau = 1/\tau_{\text{ph}}(T) + 1/\tau_{\text{eff}} \tag{A7}$$

we have

$$\tau_{\text{eff}}/\tau_{\text{ph}}(T) = kT/\tfrac{1}{2}k\Theta_D \tag{A8}$$

or

$$\tau_{\text{eff}} = 2(T/\Theta_D)\,\tau_{\text{ph}}\,. \tag{A9}$$

Holstein[36] obtains a similar result for the three-dimensional case, but with a numerical factor of $\frac{5}{2}$ instead of 2.

---

†Research supported by the National Science Foundation through the Laboratory for Research on the Structure of Matter and Grant No. GH-39303, and by the Advanced Research Projects Agency through Grant No. DAHC 15-72C-0174.

*Work submitted in partial fulfillment of the requirements for the Ph.D.

[1]L. B. Coleman, M. J. Cohen, D. J. Sandman, F. G. Yamagishi, A. F. Garito, and A. J. Heeger, Solid State Commun. 12, 1125 (1973).

[2]J. Ferraris, D. O. Cowan, V. Walatka, Jr., and J. H. Perlstein, J. Am. Chem. Soc. 95, 948 (1973).

[3]A. F. Garito and A. J. Heeger, Nobel Symp. 24, 129 (1973).

[4]A. A. Bright, A. F. Garito, and A. J. Heeger, Solid State Commun. 13, 943 (1973).

[5]P. M. Grant, R. L. Greene, G. C. Wrighton, and G. Castro, Phys. Rev. Lett. 31, 1311 (1973).

[6]M. J. Cohen, L. B. Coleman, A. F. Garito, and A. J. Heeger, Phys. Rev. B (to be published).

[7]J. H. Perlstein, J. P. Ferraris, V. V. Walatka, D. O. Cowan, and G. A. Candela, AIP Conf. Proc. 10, 1494 (1973).

[8]S. K. Khanna, E. Ehrenfreund, A. F. Garito, and A. J. Heeger, Phys. Rev. B (to be published).

[9]A. A. Bright, Ph.D. dissertation (University of Penn-

sylvania, 1973 (unpublished).
[10]P. M. Chaikin, J. F. Kwak, T. E. Jones, A. F. Garito, and A. J. Heeger, Phys. Rev. Lett. 31, 601 (1973).
[11]J. C. Scott, A. F. Garito, and A. J. Heeger (unpublished). These data were presented at the International Conference on Magnetism, Moscow, August, 1973, and at the Gatlinburg Conference on Superconductivity and Lattice Instabilities, September, 1973.
[12]E. F. Rybaczewski, A. F. Garito, and A. J. Heeger, Bull. Am. Phys. Soc. 18, 450 (1973).
[13]E. F. Rybaczewski, E. Ehrenfreund, A. F. Garito, and A. J. Heeger (unpublished). These data were presented at the Gatlinburg Conference on Superconductivity and Lattice Instabilities, September, 1973.
[14]A. J. Epstein, S. Etemad, A. F. Garito, and A. J. Heeger, Phys. Rev. B 5, 952 (1972).
[15]T. E. Phillips, T. J. Kistenmacher, J. P. Ferraris, and D. O. Cowan, Chem. Commun. 471 (1973); J. J. Daly and F. Sanz, (unpublished).
[16]J. J. Hopfield, Comments Solid State Phys. 3, 48 (1970).
[17]R. E. Peierls, *Quantum Theory of Solids* (Oxford U.P., London, 1955), p. 108.
[18]H. Fröhlich, Proc. R. Soc. A 223, 296 (1954).
[19]M. J. Rice and S. Strässler, Solid State Commun. 13, 697 (1973).
[20]J. Bardeen, Solid State Commun. 13, 357 (1973).
[21]Yu. A. Bychkov, L. P. Gorkov, and I. E. Dzyaloshinskii, Zh. Eksp. Teor. Fiz. 50, 738 (1966) [Sov. Phys.-JETP 23, 489 (1966)].
[22]D. Allender, J. W. Bray, and J. Bardeen, Phys. Rev. B 9, 119 (1974).
[23]D. E. Schafer, F. Wudl, G. A. Thomas, J. P. Ferraris, and D. O. Cowan, Solid State Commun. 14, 347 (1974).
[24]L. B. Coleman, J. A. Cohen, A. F. Garito, and A. J. Heeger, Phys. Rev. B 7, 2122 (1973).
[25]B. R. O'Connor and F. N. Jones, J. Org. Chem. 35, 2002 (1970); E. Klingsberg, J. Am. Chem. Soc. 86, 5290 (1964); D. L. Coffen, J. Q. Chambers, D. R. Williams, P. E. Garrett, and N. D. Canfield, J. Am. Chem. Soc. 93, 2258 (1971); F. Wudl, G. M. Smith, and E. J. Hufnagel, Chem. Commun. 1453 (1970).
[26]W. A. Eaton, Ph.D. thesis (University of Pennsylvania, 1967) (unpublished).
[27]B. G. Anex, Mol. Cryst. 1, 1 (1966); J. C. Barnes and A. J. Thompson, J. Sci. Instrum. 44, 577 (1967).
[28]H. Kuroda, S. Hiroma, and H. Akamatu, Bull. Chem. Soc. Jap. 41, 2855 (1968); Bull. Chem. Soc. Jap. 44, 9 (1971).
[29]D. B. Tanner, C. Jacobsen, A. F. Garito, and A. J. Heeger, Phys. Rev. Lett. 32, 1301 (1974).
[30]See, for example, F. Wooten, *Optical Properties of Solids* (Academic, New York, 1972), Chap. 3.
[31]P. R. Bevington, *Data Reduction and Error Analysis for the Physical Sciences* (McGraw-Hill, New York, 1969), p. 212.
[32]B. G. Anex and W. T. Simpson, Rev. Mod. Phys. 32, 466 (1960).
[33]The data presented by J. B. Torrance at the Gatlinburg Conference on Superconductivity and Lattice Instabilities, September, 1973, show a very broad maximum near 0.3 eV, or 3.6 μm.
[34]M. J. Rice and S. Strässler, report of work prior to publication.
[35]P. A. Lee, T. M. Rice, and P. W. Anderson, Solid State Commun. 14, 703 (1974).
[36]T. Holstein, Phys. Rev. 96, 535 (1954).
[37]T. Wei, S. Etemad, A. F. Garito, and A. J. Heeger, Phys. Lett. A 45, 269 (1973).
[38]C. W. Chu, J. M. E. Harper, T. H. Geballe, and R. L. Greene, Phys. Rev. Lett. 31, 1491 (1973).
[39]R. L. Greene (private communication).
[40]H. E. Bennett and J. M. Bennett, in *Optical Properties and Electronic Structure of Metals and Alloys*, edited by F. Abelès (North-Holland, Amsterdam, 1966), p. 175.
[41]P. Coppins and R. Blushing (private communication).
[42]G. Stucky (private communication).
[43]M. B. Barmatz, L. R. Testardi, A. F. Garito, and A. J. Heeger (unpublished).
[44]A. J. Heeger and A. F. Garito, Rev. Mod. Phys. (to be published).
[45]C. G. Kuper, Proc. R. Soc. A 227, 214 (1955).
[46]R. A. Craven, M. B. Salomon, G. DePasquali, R. M. Herman, G. Stucky, and A. Schultz, Phys. Rev. Lett. 32, 769 (1974).
[47]P. A. Lee, T. M. Rice, and P. W. Anderson, Phys. Rev. Lett. 31, 462 (1973).